1993

Development of a rapidly computable descriptor of prostate tissue temperature during transurethral conductive heat therapy for benign prostate hyperplasia

U H. Patel

Charles F. Babbs
Purdue University, babbs@purdue.edu

Modeling

Development of a rapidly computable descriptor of prostate tissue temperature during transurethral conductive heat therapy for benign prostate hyperplasia

U. H. PATEL C. F. BABBS

Biomedical Engineering Center, Purdue University, West Lafayette, Indiana, USA.

Abstract—Benign prostate hyperplasia (BPH) is a condition in older men in which the mass of tissue in the prostate gland gradually increases over the course of many years, ultimately leading to urinary outflow obstruction. Current treatment of this condition is to surgically remove the obstructing tissue. One novel alternative therapy being studied is transurethral thermocoagulation of excessive prostatic mass. In this approach, a heat emitting catheter is placed in the prostatic urethra, and the intraprostatic segment of the catheter is heated to temperatures above 60 ^{o}C for one hour. Two dimensional cylindrical coordinate computer simulations of this treatment modality were run to model resultant temperature distributions within the prostate gland and surrounding tissues. The simulations revealed that resultant tissue temperature changes were related directly to the power delivered to the catheter and inversely to the rate of blood perfusion. Further analysis of the temperature profiles produced a rapidly computable predictor of tissue temperature in the radial dimension. Using the predictor, a 'kill radius' around the prostatic urethra can be easily computed online, during treatment, from clinically available data: the catheter power and catheter temperature. The computed kill radius may serve as a useful predictor of the extent of thermal devitalization of unwanted obstructing tissue and the long term success of the treatment in relieving urinary outflow obstruction without surgery.

Key words—Benign prostatic hyperplasia, BPH, Conductive heating, Prostate gland, Thermocoagulation

Medical & Biological Engineering & Computing 1993, 31, 475-481

Supported in part by grant CA-38144 from the National Cancer Institute, US Public Health Service, Bethesda, Maryland, USA.

1 Introduction

Benign prostatic hyperplasia (BPH) is a condition characterized by non-malignant proliferation of tissue within the capsule of the prostate gland, ultimately leading to obstruction of urinary flow through the prostatic urethra. BPH is estimated to affect about 50 percent of men over the age of 60 years; in men over 80 years of age, 80 percent are affected (HULBERT, 1989).

The traditional treatment for urinary obstruction due to BPH is the surgical removal of hyperplastic prostatic tissue, usually by endoscopic transurethral reaction of the prostate (TURP). In 1983, approximately 357,000 men in the USA underwent prostatic resection, either by transurethral or by abdominal approaches (ERCOLE, 1989). In a multi-center study, MEBUST *et al.* (1989) found that, although the surgical mortality due to transurethral resection was low (0-2 per cent), the morbidity of the procedure (failure to void, bleeding requiring transfusions, clot retention, and genitourinary infections) was 18 per cent. For patients older than 80 years, the morbidity was 22.6 per cent. When the duration of procedure was greater than 90 min, intra-operative bleeding requiring a blood transfusion occurred in 7-3 percent of cases. The cost of TURP for each patient totals about $10,000, owing to the need for hospitalization, surgeon's and anesthetist's fees and operating room time (CASTANEDA *et al.,* 1987).

A variety of alternatives to TURP are being investigated. Medical treatment of BPH with endocrine and alpha-adrenergic blocker therapy has been somewhat successful; however, the effects are reported to be temporary (ERCOLE, 1989). For patients in whom surgery is not indicated, long term intra-urethral prostheses have been tried to treat urinary flow obstruction (VINCENTE *et al.,* 1989), but these devices promoted an undesirable incidence of urinary tract infection. Another procedure being investigated is prostatic urethroplasty with a balloon catheter (CASTANEDA *et al.,* 1987). Reported results from this procedure have been mixed (GONZALEZ *et al.,* 1989; HERRERA *et al.,* 1989; MACHAN et *al.,* 1989). Complications include initial hematuria, which usually clears in 24 hours, severe delayed hemorrhage, and acute urinary retention (CASTANEDA, 1989). Microwave hyperthermia is also under investigation as an alternative to TURP. As with balloon dilatation, the results have been mixed (SAPOZTNK *et al.,* 1990; STROHMAIER *et al.,* 1990). Short term complications of microwave hyperthermia include hematuria, bladder spasm, and dysuria.

This paper describes theoretical studies of a potential new modality for the minimally invasive treatment of BPH; transurethral thermocoagulation of the prostate. In contrast to hyperthermia therapy at 42-46 ^{o}C generated by transurethral microwave techniques (SAPOZINK *et al.,* 1990), thermocoagulation involves the deliberate generation of high temperatures (> 60 ^{o}C for 1 hr) sufficient to cause coagulative necrosis of treated periurethral tissue. The goal is to coagulate an annular sleeve of periurethral prostatic tissue, which will subsequently be resorbed with minimal bleeding, followed by regeneration of the urethral epithelium and relief of urinary outflow obstruction. Technology currently under development for transurethral thermocoagulation includes a 7-10 Fr (2.2-3.2 mm diameter) catheter containing a wire wound, electrically heated resistor near the catheter tip (Fig. 1). Catheters may be selected with the heating element ranging from 3 to 4 cm in length to match the ultrasonically measured prostatic dimensions in individual patients. A high thermal conductivity elastomer is used to couple the heating element to the polyethylene covering. To monitor and control the temperature of the heating element, a high

precision thermistor is located at the center of the heating element. In operation, the catheter is placed in the prostatic urethra with the aid of transrectal ultrasonography to verify the catheter position. Direct current is then applied to the catheter and the power is adjusted via computer control such that the internal catheter temperature is held constant. Heat is delivered to the tissue by thermal conduction only, as in other recently developed conductive heating techniques (DEFORD *et al.,* 1991).

Preliminary trials (unpublished study) using this procedure in the canine model have been encouraging. The internal catheter temperatures, ranging from 59 to 87 ^{o}C were generated for 20-60 min. Histopathologic findings immediately following heat treatment revealed coagulative necrosis extending 1 to 3 cm radially from the catheter edge into periurethral stroma and glandular elements. Treated prostate glands studied 2, 4, or 8 weeks after thermocoagulation by retrograde urethrography and light microscopy exhibited a consistent pattern of edema and non-infective inflammation with minimal luminal narrowing at 2 weeks; followed by resolution of the inflammatory response, re-epithelialization, widening of the prostatic urethra, and atrophy of the periurethral prostatic glands, with maintenance of the normal architecture of periurethral connective tissue.

To further refine the technique for clinical use, accurate control of catheter placement and heat delivery are necessary, so as to not damage normal tissues, such as the urinary sphincter. This paper describes the use of a computer model to predict temperature distributions created by conductive thermocoagulation of the prostate and to predict the 'kill radius' within which clearly cytotoxic temperatures are achieved. A two dimensional cylindrical coordinate model, very similar to one previously described (PATEL *et al.,* 1991), was used, so that temperature gradients could be evaluated in both radial and longitudinal dimensions. Evaluation of the simulated temperature distribution led to the development of a rapidly computable predictor of periprostatic temperature distributions.

2 Computational methods

2.1 *Theory*

The computational formulae used in this study were based on the bioheat transfer equation first described by PENNES (1948) for a small control volume of tissue:

$$\dot{q}_{met} + P + K\nabla^2 T + c_b \omega_b (T_b - T) = \rho c \frac{\partial T}{\partial t}, \qquad (1)$$

where $\dot{q}_{met}$ is the specific rate of metabolic heat production, P is the power density delivered to tissue, K is the tissue thermal conductivity, T is the temperature of tissue, c_b is the specific heat of blood, ω_b is the specific flow rate of blood in capillaries, T_b is the temperature of blood, ρ is the mass density of tissue, c is the specific heat of tissue, and t is time. The control volume is small enough that all thermal properties within it are uniform. For an interstitial, conductive heating modality at steady state, metabolic heat production is small compared with other terms

(DEFORD, 1989), power is not directly delivered to the tissue, and $\partial T/\partial t \to 0$. Thus, equation (1) simplifies to

$$K\nabla^2 T + c_b\omega_b(T_b - T) = 0. \qquad (2)$$

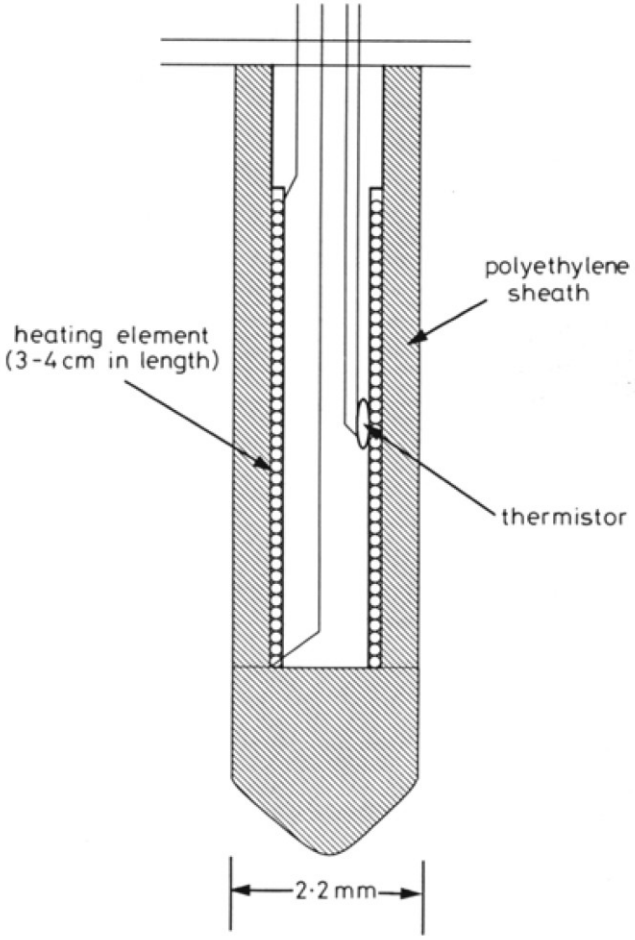

Fig. 1 *Sketch of tip of conductive heating catheter used for transurethral heating of canine prostate.*

2.2 *Modeled volume*

The prostate and surrounding tissue were modeled in a cylindrical space, assuming radial symmetry. Fig. 2 shows a sketch of the model space in cross section. The urethra was modeled as a potential space occupied by the heat emitting catheter along the central axis. The prostate region was modeled as the middle elliptical portion of the cylinder. The bladder was modeled as the top of the cylinder containing fluid at 37 ^{o}C. This section tapered down to the urethra. Just below the prostate, the external, voluntary sphincter was modeled as ring of tissue 1 cm thick

with a radius of 2 cm. The remaining volume of the cylinder was modeled as surrounding connective tissue. The outer edge of the cylinder, x = 3 cm, was clamped to arterial blood temperature, 37 ^{o}C. The bottom of the cylinder was also clamped to arterial blood temperature.

The control volumes in this model were similar to the control volumes described by PATEL *et al.* (1991) for computer simulation of hyperthermia therapy in brain tumors. Except for the central axis, each control volume was a ring of tissue. Heat conduction occurred radially between control volumes of the same height and longitudinally between control volumes of the same radius. In this study, each ring had a height *dz* of 0.04 cm and a width *dr* of 0.01 cm. Thus, the entire model space contained 60000 control volumes. Even though this was a two dimensional model, incorporating radial symmetry for simplicity, the large number and small sizes of the control volumes were necessary to obtain valid numerical results in the presence of the steep thermal gradients, *dT/dr*, associated with conductive heating.

2.3 *Computational formulae and simulations*

The computational formulae and the methods were identical to those previously derived (PATEL *et al.,* 1991). The following shows the computational formula used to obtain an iterative solution to the steady-state bioheat transfer equation for the temperature rise above arterial blood temperature (θ_C) for the center control volume shown in Fig. 3, which represents a typical ring of tissue:

$$\theta_C = \frac{\theta_I\left[\frac{K_{IC}}{dr^2}\left(1-\frac{dr}{2r}\right)\right] - \theta_O\left[\frac{K_{CO}}{dr^2}\left(1+\frac{dr}{2r}\right)\right] + \theta_U\frac{K_{UC}}{dz^2} - \theta_L\frac{K_{CL}}{dz^2}}{c_b w_b + \frac{K_{IC}}{dr^2}\left(1-\frac{dr}{2r}\right) + \frac{K_{CO}}{dr^2}\left(1+\frac{dr}{2r}\right) + \frac{K_{UC}}{dz^2} + \frac{K_{CL}}{dz^2}} \quad (3)$$

θ_x is the temperature rise above arterial blood temperature for control volume x, K_{xy} is the interface thermal conductivity between control volumes x and y (DeFORD *et al.,* 1990), *r* is radial distance to the center control volume, c_b is the specific heat of blood and ω_b is the blood perfusion in the tissue control volume. The subscripts *C, I, O, U* and *L* are as defined in Fig. 3. For control volumes containing the heating element, a power deposition term was added to the numerator and the perfusion term $c_b\omega_b$ in the denominator was zero. For other areas of the model space, in which there would be no blood flow (i.e. the catheter components, bladder fluid), the perfusion term was also zero.

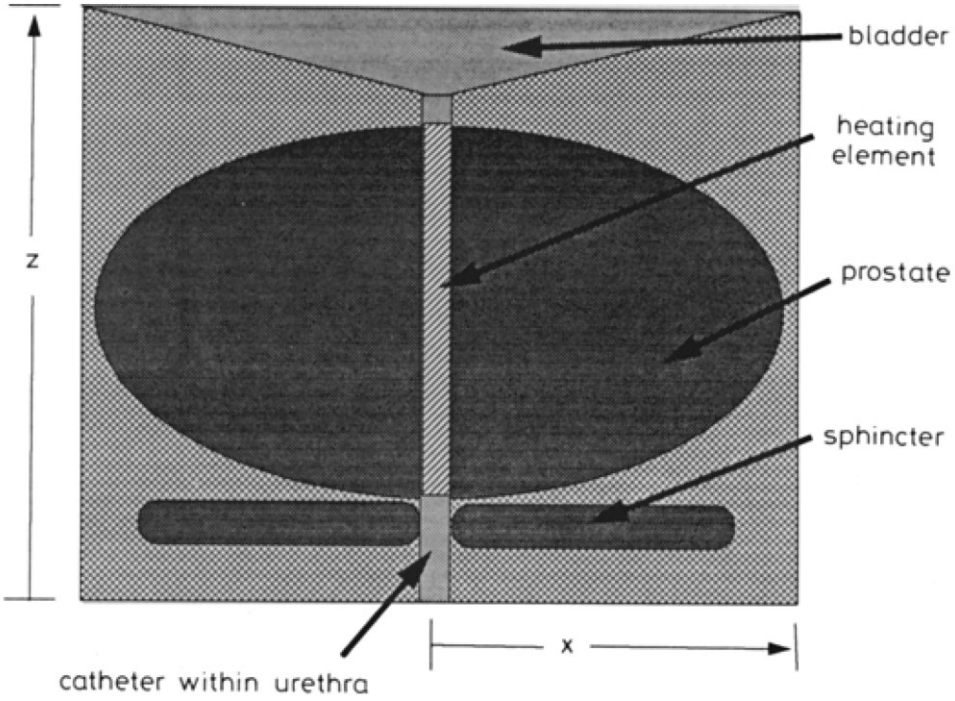

Fig. 2 *Modeled cylindrical volume shown in cross-section. The cylinder has a height of 5 cm and a radius of 3 cm.*

Values for the specific heat of blood (3642.6 J/(kg ^{o}C) and for tissue thermal conductivity (0.564 W/(m ^{o}C)) were taken from the literature (ALBRITTON, 1952; COOPER and TREZEK, 1971). The thermal conductivities of the catheter components were obtained from the literature (INCROPERA and DEWITT, 1981), or measured experimentally, as described previously (PATEL *et al.,* 1991).

A modified Gauss-Seidel method was used to solve the derived bioheat transfer equations for each control volume iteratively, beginning with an initial condition of $\theta = 0$ everywhere. The simulations were run on the Ardent Titan-P3 computer (Ardent Computer Corp.) which was running at 60 MIPS. Each simulation required approximately 1-3 hours to complete.

The output from a simulation was a file containing the steady-state temperature rise for each control volume for given conditions of catheter power and tissue perfusion. Contour plots were generated from these data and the thermal profiles were evaluated. Temperature profiles from a total of 40 simulations were analyzed. Catheter power was varied from 0.5 to 1.0 W/cm and prostate blood perfusion was varied from 0.05 to 0.7ml/min/g. In all simulations, perfusion in the sphincter was 0.3 ml/min/g and all other surrounding tissue perfusion was 0.1 ml/min/g. Thus, a large family of simulations was performed, the analysis of which revealed helpful regularities in the thermal responses to this geometrically simple heat treatment modality. In turn, it was possible to derive a much simpler predictor of tissue temperature for use in clinical work than the complete bioheat equation.

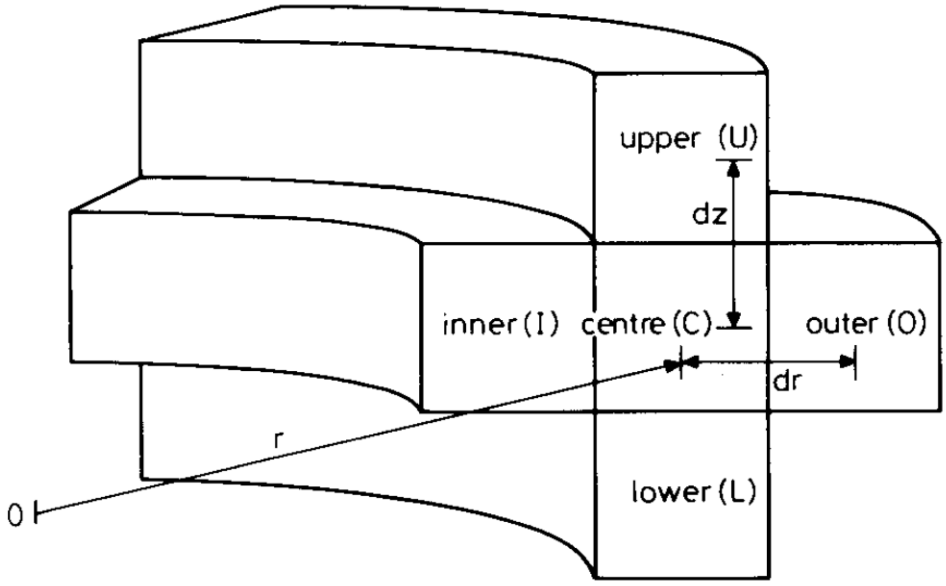

Fig. 3 *Diagram showing heat conduction between interior control volumes center(C), inner (I), outer (O), upper (U), and lower (L). Heat conduction occurs radially between control volumes, I, C and O, and occurs longitudinally between control volumes U, C, and L. Each control volume has width dr and height dz.*

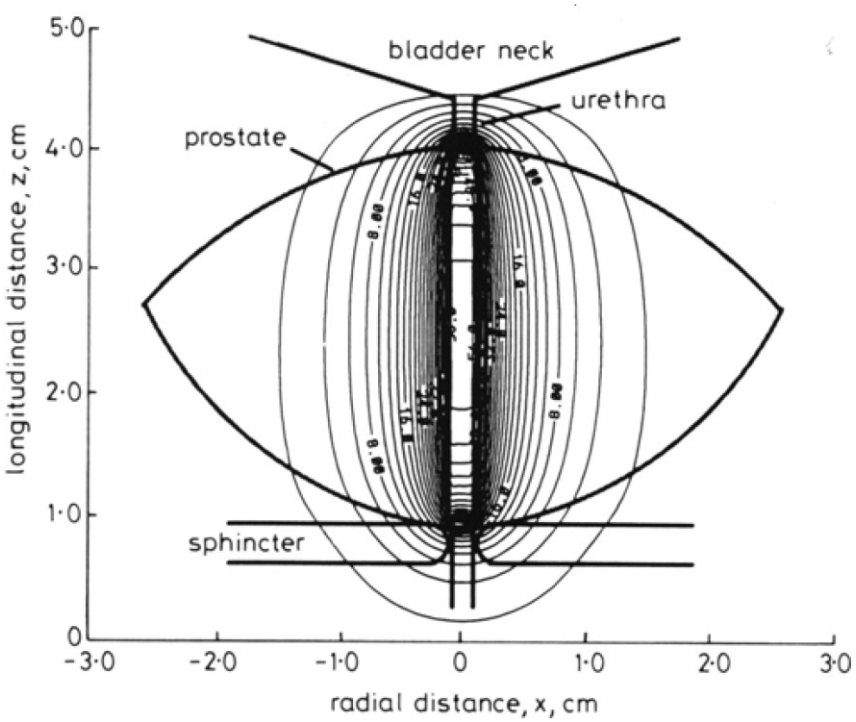

Fig. 4 *Contour plot showing the thermal profile produced from a simulation with a catheter power of 0.7 W/cm and a prostate blood perfusion of 0.2 ml/min/g. Perfusion in the sphincter region was 0.3 ml/min/g. All other tissue was modeled with a perfusion of 0.1 ml/min/g. Tissue thermal conductivity was 0.564 W/(m ^{o}C), heating element thermal conductivity was 12.0 W/(m ^{o}C), and catheter sheath thermal conductivity was 0.4 W/(m ^{o}C). Simulations had a radial resolution of 0.01 cm and longitudinal resolution of 0.04 cm. Each contour represents a 2 ^{o}C change in temperature. Numbers on contours represent the temperature above arterial blood temperature.*

3 Results and predictor development

3.1 *Simulation results*

Fig. 4 shows a contour plot of steady-state temperature elevations obtained in a typical simulation. Superimposed on the plot is the outline of the various features in the modeled volume. The decay of temperature with radial distance, x, from the catheter edge was similar for most central levels, z, along the heating element. Steep longitudinal temperature gradients developed only at the ends of the heating element. Fig. 5 shows a plot of radial temperature profiles in a plane containing the midpoint of the heating element (z = 2.5 cm in Fig. 4) from five simulations of different catheter power (0.5-1.0 W/cm) and a constant blood perfusion of 0.2 ml/min/g. The radial distance x in this plot is zero at the center of the catheter.

The temperature profiles obtained were dependent on catheter power. To normalize the results, the ratio of temperature rise above arterial blood temperature to catheter power in W/cm was plotted against radial distance (Fig. 6a), and the curves collapsed to a single curve. Fig. 6b shows this normalization for all perfusion levels simulated. Each curve in Fig. 6b represents five different power levels and one perfusion level. The relationship shown in Fig. 6b was then used to develop a predictor of radial tissue temperature that would require far less computation time than the solution of the entire bioheat equation for 60000 control volumes.

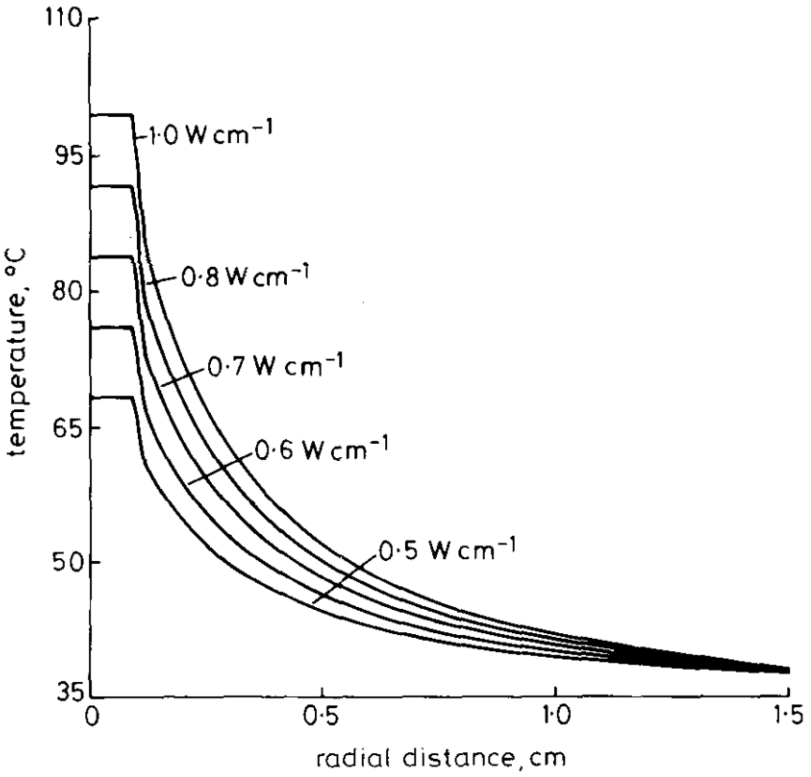

Fig. 5 *Radial temperature profiles from five computer simulations with catheter powers of 0.5, 0.6, 0.7, 0.8 and 1.0 W/cm and prostate blood perfusion of 0.2 ml/min/g. The topmost profile is from a simulation with a catheter power of 1.0 W/cm. Other details are similar to Fig. 4.*

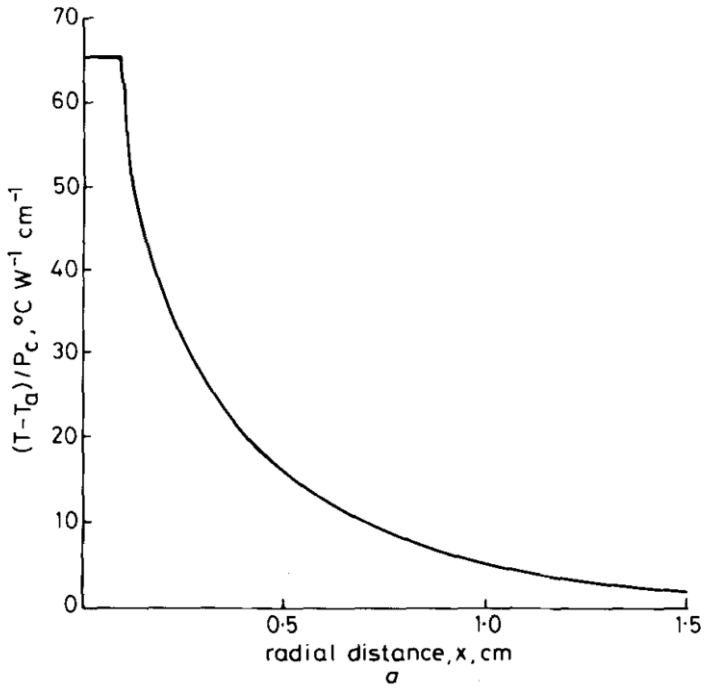

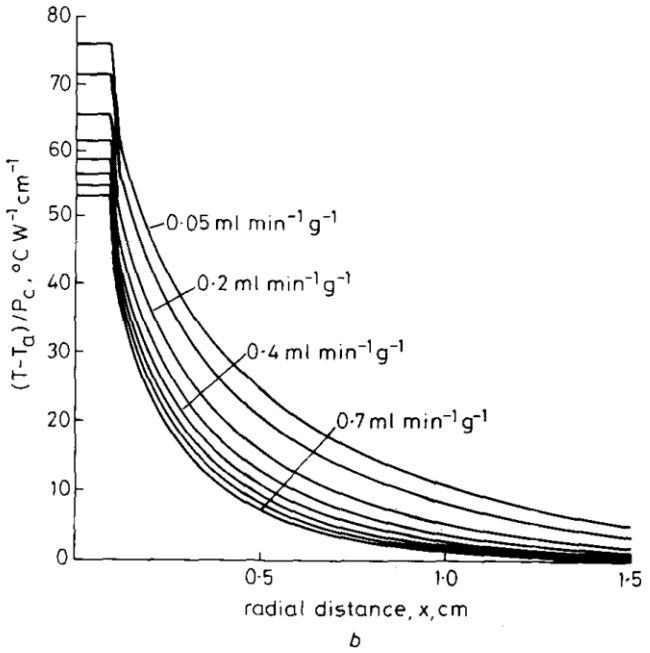

Fig 6. *(a) Plot of temperature rise above arterial temperature divided by catheter power P_c against radial distance from the catheter center. Data are shown from the five simulations described in Fig. 5. (b) The same plot as (a), but data are shown for all perfusion levels simulated: 0.05, 0.1, 0.2, 0.3, 0.4, 0.5, 0.6 and 0.7 ml/min/ g. The topmost curve represents simulations with a prostate blood perfusion of 0.05 ml/min/g. The lowest curve represents simulations with a prostate blood perfusion of 0.7 ml/min/g.*

3.2 *Predictor development*

The curves shown in Fig. 6b were offset from each other due to different levels of perfusion. Thus, an equation governing the behavior of the curves would have the following form:

$$\frac{T - T_a}{P_c} = f(\omega, r) \tag{4}$$

P_c is catheter power in W/cm, $T - T_a$ is the tissue temperature rise above arterial blood temperature in ^oC, r is the distance away from the catheter edge ($x–r_c$) in cm, ω is the prostate blood perfusion in ml/min/g, and $f(\omega, r)$ is a function dependent on perfusion and distance in $^oC/(W\text{-cm})$. As the curves in Fig. 6b were quasi-exponential in nature, $f(\omega, r)$ was assumed to be an exponential function. Thus

$$f(\omega, r) = e^{g(\omega, r)} \tag{5}$$

or

$$g(\omega, r) = \ln\left(\frac{T - T_a}{P_c}\right). \tag{6}$$

Therefore, to find $g(\omega, r)$, $\ln((T - T_a)/P_c)$ was plotted against distance r for all simulated perfusion levels (Fig. 7). For $r > 0.5$ cm, a nearly linear family of curves was obtained, and for $r < 0.5$ cm, the curves appeared to be second-order. Thus, to approximate $f(\omega, r)$, the radial dimension was divided into two regions; near field ($r < 0.5$ cm) and far field ($r > 0.5$ cm). For the near field, $f(\omega, r)$ was of the form $ar^2 + br + c$, where the coefficients a, b, and c were dependent on perfusion. Using second-order regression analysis, the coefficients a, b, and c were found for each perfusion level that was simulated. Table 1 summarizes the results showing the values of the coefficients. Next the coefficients a, b and c were plotted against perfusion and an additional regression analysis was performed to obtain quadratic equations to describe the near field coefficients in terms of perfusion ω.

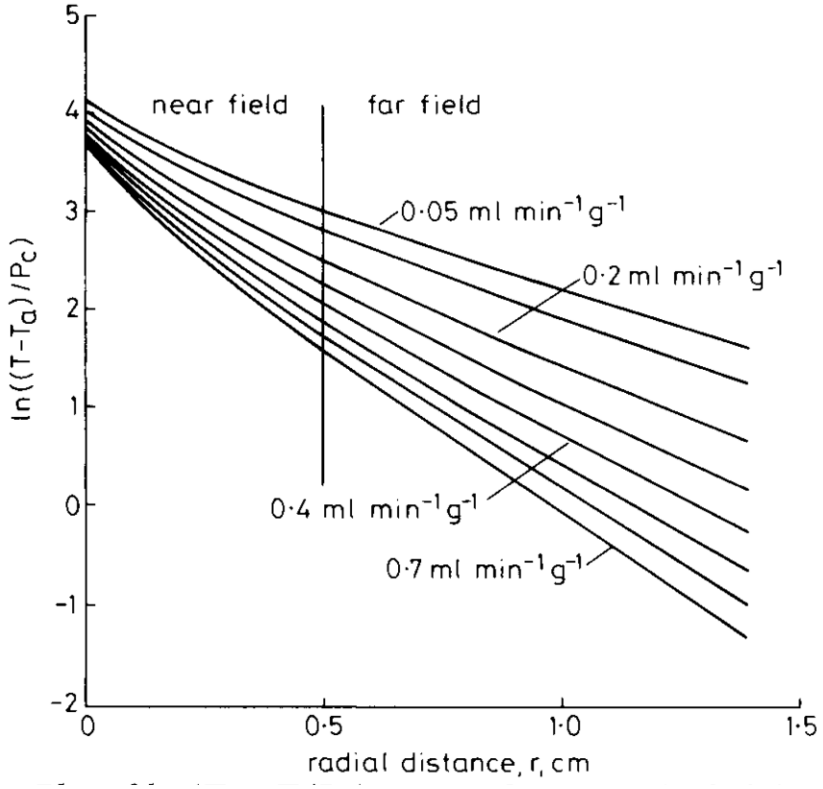

Fig. 7 *Plot of $\ln((T - T_a)/P_c)$ against distance, r (radial distance away from catheter edge). The near field region shows curves that are second-order in nature, and the far field shows curves that are linear in nature. The topmost curve represents simulations with a prostate blood perfusion of 0.05 ml/min/g. The lowest curve represents simulations with a prostate blood perfusion of 0.7 ml/min/g.*

Table 1 Coefficient values for near and far field estimators; r^2 denotes the coefficient of determination for the least-squares fitted curve or line.

perfusion ml min^{-1} g^{-1}	near field				far field		
	a	b	c	r^2	m	b	r^2
0·05	1·59	−2·98	4·12	1·00	−1·54	3·77	1·00
0·1	1·67	−3·27	4·05	1·00	−1·72	3·64	1·00
0·2	1·77	−3·71	3·94	1·00	−2·05	3·50	1·00
0·3	1·84	−4·07	3·86	1·00	−2·34	3·40	1·00
0·4	1·89	−4·37	3·80	1·00	−2·62	3·34	1·00
0·5	1·94	−4·64	3·74	1·00	−2·83	3·25	1·00
0·6	1·97	−4·88	3·70	1·00	−3·03	3·21	1·00
0·7	2·00	−5·10	3·66	1·00	−3·23	3·16	1·00

Table 2 Coefficient estimation equations in terms of perfusion; r^2 is the coefficient of determination for the least-squares fitted curves.

near-field coefficients	
$a = -0{\cdot}81\omega^2 + 1{\cdot}20\omega + 1{\cdot}55$	$r^2 = 0{\cdot}99$
$b = 2{\cdot}45\omega^2 - 5{\cdot}01\omega - 2{\cdot}77$	$r^2 = 1{\cdot}00$
$c = 0{\cdot}75\omega^2 - 1{\cdot}24\omega + 4{\cdot}17$	$r^2 = 1{\cdot}00$
far-field coefficients	
$m = 1{\cdot}52\omega^2 - 3{\cdot}71\omega - 1{\cdot}36$	$r^2 = 1{\cdot}00$
$b = 1{\cdot}12\omega^2 - 1{\cdot}71\omega + 3{\cdot}82$	$r^2 = 0{\cdot}99$

For the far field, f(ω, r) was of the form, mr + b, where the coefficients m and b were dependent on perfusion. Using linear regression analysis, the coefficients m and b were obtained (Table 1). Then the coefficients m and b were plotted against perfusion and an additional regression analysis was performed to obtain quadratic equations to describe the far field coefficient values in terms of perfusion.

Table 2 summarizes the second-order fits for the coefficient values in terms of perfusion. Substituting the functions f(ω, r) and g(ω, r) in Equation 5 for the near field and far field, respectively, the estimators of Equations 7 and 8 were obtained:

$$\begin{aligned} T - T_a = P_c \exp\,&(-0{\cdot}81\omega^2 + 1{\cdot}20\omega + 1{\cdot}55)r^2 \\ &+ (2{\cdot}45\omega^2 - 5{\cdot}01\omega - 2{\cdot}77)r \\ &+ (0{\cdot}75\omega^2 - 1{\cdot}24\omega + 4{\cdot}17) \end{aligned} \tag{7}$$

$$T - T_a = P_c \exp(1{\cdot}52\omega^2 - 3{\cdot}71\omega - 1{\cdot}36)r + (1{\cdot}12\omega^2 - 1{\cdot}71\omega + 3{\cdot}82) \quad (8)$$

Equation (7) is a near field estimator, and Equation (8) is the far field estimator. These estimators could be used to find tissue temperature rise at any distance in the radial direction from the catheter edge within the heating space.

It is important to note that these estimators do not give valid answers for perfusion levels greater than 1.0 ml/min/g. If perfusions are greater than 1.0 ml/min/g, predicted temperatures are overestimated. For prostatic blood perfusion levels modeled within the physiological range, 0.15 0.79 ml/min/g (ANDERSON *et al.,* 1967; HAEENER and LIAVAG, 1969), temperature estimates are accurate. Figs. 8a and 8b present three dimensional plots showing the behavior of the near and far field estimators as a function of prostatic blood perfusions less than 1.0 ml/min/g and of radial distances less than 2.5 cm.

The temperature estimators of Equations 7 and 8 are not clinically useful unless perfusion can also be estimated. DEFORD *et al.* (1992) showed that, in conductive heating, tissue perfusion could be estimated if catheter power and catheter temperature rise were known. Fig. 9 shows a plot of perfusion against the ratio of catheter power to catheter temperature rise above arterial blood temperature (defined as $\sigma = P_c/[T_c - T_a]$) obtained from the simulations run in this study. Each triangle represents five overlapping data points at different power levels. Second-order regression analysis yielded the following equation that predicts perfusion in terms of

$$\omega = 12665{\cdot}1\sigma^2 - 292{\cdot}5\sigma + 1{\cdot}7 \quad (9)$$

Positive values for ω are obtained only when σ is greater than 0.0115 W/(cm ^{o}C). In unpublished experimental studies, σ has been well above this value. Thus, by calculating perfusion with Equation 9 in terms of clinical variables that can be readily measured online (catheter power and catheter temperature), Equations 7 and 8 can then be used to predict prostatic tissue temperature at any distance radially away from the catheter edge.

Conversely, it is possible to predict the radial distance from the catheter within which thermocoagulation is expected to occur. From the work of JAIN and DUDAR (1983), we can expect coagulation necrosis to occur in tissue raised to 47 ^{o}C or more for a minimum of 50 min. In unpublished animal studies, the 47 ^{o}C contour appears to circumscribe the zone of grossly and histologically observable necrosis of prostatic tissue after transurethral thermocoagulation in the dog model. Solving Equation 8 for r at 47 ^{o}C we obtain

$$r_{47} = \frac{\ln(47 - 37) - \ln(P_c) - 1{\cdot}12\omega^2 + 1{\cdot}71\omega - 3{\cdot}82}{1{\cdot}52\omega^2 - 3{\cdot}71\omega - 1{\cdot}36} \quad (10)$$

for r_{47} in the far field. Similar analysis can be performed to obtain r_{47} for the near field. If the calculated value for r_{47} is less than 0.5 cm, then r_{47} should be recalculated using the near field estimator equation. Thus, the extent of thermocoagulation can be predicted by online measurements of catheter power and temperature, based on the prior computer solutions of the bioheat transfer equation presented here. If the predicted kill radius is insufficient, then the power can be increased during therapy to achieve a target therapeutic coagulation radius. Conversely, if the computed kill radius is too large, the power can be decreased.

3.3. *Predictor verification*

To validate the accuracy of the predictor, tissue temperatures calculated by the predictor were compared with those obtained from computer simulations. This comparison was performed for two cases: the first, in which catheter power was high and perfusion was low, and the second, in which catheter power was low and perfusion was high. In the first case the computer simulation produced a large thermal gradient, and in the second case the computer simulation produced a small thermal gradient. Fig. 10 shows plots of radial thermal profiles produced from computer simulations (solid lines) and the radial thermal profiles calculated using the tissue temperature estimators from Equations 7-9 (broken lines). The upper curves represent profiles using a catheter power of 1.0 W/cm and a tissue perfusion of 0.05 ml/min/g, and the lower curves represent profiles using a catheter power of 0.5 W/cm and a tissue perfusion of 0.7 ml/min/g. In the first case the r_{47} was 1.02 cm simulated against 1.01 cm predicted; in the second case the r_{47} was 0.24 cm simulated against 0.24 cm predicted.

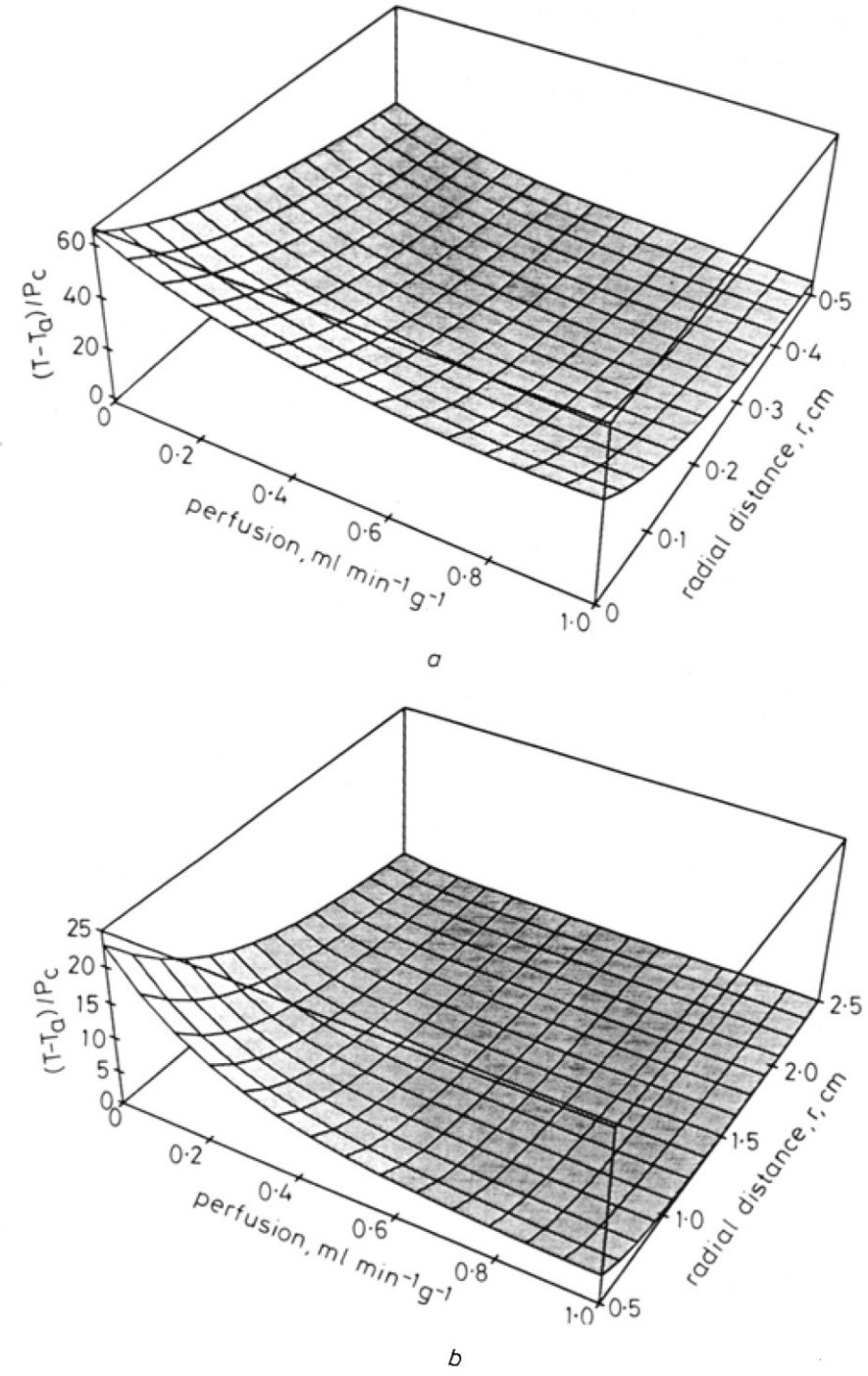

Fig. 8 *(a) Three dimensional plot showing behavior of the near field estimator, Equation 7. The plot shows the calculated value of* $(T - T_a)/P_c$ *in* $^oC/(W\ cm)$ *for* $0 \le r \le 0.5$ *and* $0 \le \omega \le 1.0$ *ml/min/g. (b) Three dimensional plot showing the behavior of the far field estimator, Equation 8. The plot shows the calculated value of* $(T - T_a)/P_c$ *in* $^oC/(W\ cm)$ *for* $0.5 \le r \le 2.5$ *cm and* $0 \le \omega \le 1.0$ *ml/min/g. The plot indicates that estimator is a smooth continuous function even for values of r greater than 1.5 cm.*

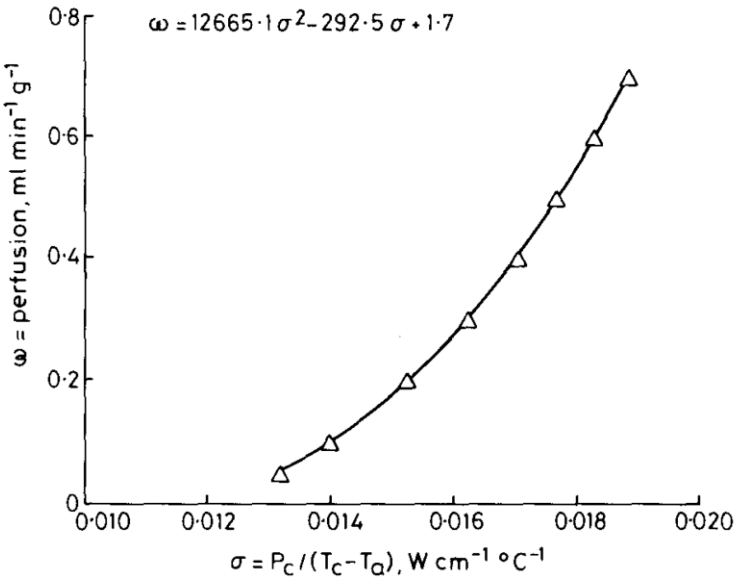

Fig. 9 *Plot of tissue perfusion against catheter power divided by catheter temperature rise. Each triangle represents five power levels. The curve drawn through the data was generated using the perfusion estimation equation (Equation 9).*

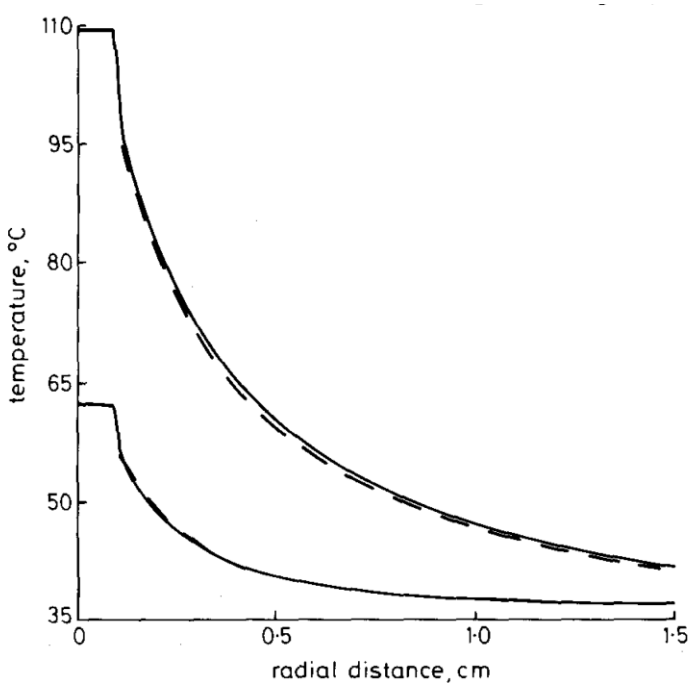

Fig. 10 *Temperature profiles generated from a computer simulation (solid line) and temperature predictor (broken line). For the upper curves, starting and 110 °C catheter power was 1.0 W/cm and perfusion was 0.05 ml/min/g. For the lower curves, catheter power was 0.5 W/cm and perfusion was 0.7 ml/min/g.*

4 Discussion

This paper presents the development of a rapidly computable, online tissue estimator for prostatic tissue during transurethral prostatic thermocoagulation. The model used to develop the predictor assumed that the geometry of the prostate was symmetrical around the urethra, the thermal properties were uniform, and tissue perfusion was homogeneous within the prostate. Provided that the thermal conductivities of the prostate and surrounding tissue are of the same order of magnitude, the assumption of a cylindrical prostate as opposed to a lobular prostate should have no effect on predictor accuracy.

The accuracy of prediction is also dependent on the accuracy of the perfusion estimate. Sensitivity analysis showed that, if perfusion is estimated to within 25 per cent of the actual value, r_{47} is within 0.7 mm of the actual value as calculated by Equation 10. DEFORD *et al.* (1992) showed that perfusion inhomogeneities should not be a factor in temperature predictor accuracy as long as variations are less than 25 per cent. Finally, this model also assumes that the catheter is placed completely within the prostatic urethra. If the catheter was misplaced within the bladder and the bladder contained urine, the power required to heat the catheter would increase due to convective heat losses in the bladder. Such a situation would cause the predicted temperatures to be underestimated. Thus, accurate placement of the catheter is necessary for the predictor to estimate temperatures properly.

This predictor has the ability to estimate mid-plane tissue temperature at any radial distance from the catheter. If desired, a similar technique to that used in this study could be supplied to develop a predictor for temperatures in the longitudinal direction. Tissue temperatures could be predicted online in major regions of the prostate and important periprostatic tissues. Knowledge of the expected thermal profiles could then be used to adjust catheter power so as to achieve a desired therapeutic effect. Thus, conductive heat could be applied effectively to the prostate to create a desired radius of thermocoagulation (r_{47}) sufficient to relieve obstructive symptoms, after resorption of the coagulated tissues. The most suitable r_{47} value could be readily learned from clinical experience. Then subsequent patients could be treated with sufficient power, adjusted moment by moment during treatment, to produce the prescribed r_{47}. In this way, formulae derived would allow physicians to write in advance a geometric prescription for thermocoagulation of the prostate.

References

ALBRITTON, E. C. (1952) *Standard values in blood.* W. B. Saunders Co., New York.

ANDERSON, L., DAHN, I., NELSON, C. and NORGEN, A. (1967) Method for measuring prostatic blood flow with Xenon in the dog. *Investigat. Urol.,* 5, 140-148.

CASTANEDA, F., REDDY, P.K., HULBERT, J. C., LUND, G., LETOURNEAU, J. G., WASSERMAN, N., HUNTER, O. W., CASTANEDAZUNIGA, W. R. and AMPLATZ, K. (1987) Retrograde prostatic urethroplasty with balloon catheter. *Sems. in Intervent. Radiol.,* **4,** 115-121.

CASTANEDA, F. (1989) Prostatic urethroplasty complications. *Ibid.,* 6, 79-81.

COOPER, T. E. and TREZEK, G. J. (1971) Correlation of thermal properties of some human tissue with water content. *Aerospace Med.,* 42, 24-27.

DEFORD, J. A. (1989) On-line estimation and control of minimum tumor temperatures during interstitial brain hyperthermia. PhD Dissertation Purdue University, West Lafayette, Indiana.

DEFORD, J. A., BABBS, C. F., PATEL, U. H., FEARNOT, N. E., MARCHOSKY, J. A. and MORAN, C. J. (1990) Accuracy and precision of computer-simulated tissue temperatures in individual human intracranial tumours treated with interstitial hyperthermia. *Int. J. Hyperthermia,* 6, 755-770.

DEFORD, J. A., BABBS, C. F., PATEL, U. H., BLEYER, M. W., MARCHOSKY, J. A. and Moran, C. J. (1991) Effective estimation and computer control of minimum tumour temperature during conductive interstitial hyperthermia. *Ibid.,* 7, 441-453.

DEFORD, J. A. BABBS, C. F. and PATEL, U. H. (1992) Droop: a rapidly computable descriptor of local minimum tissue temperature during conductive interstitial hyperthermia. *Med. & Biol. Eng. & Comput.,* 30, 333-342.

ERCOLE, C. J. (1989) Surgical and medical therapy of benign prostatic hyperplasia. *Sems. in Intervent. Radiol.,* 6, 97-101.

GONZALEZ, J. A., GANESH, D. L. and BOLONG, D. T. (1989) Prostatic urethroplasty results at William Beaumont Hospital. *Ibid.,* 6, 57-60.

HAFFNER, J. F. and LIAVAG, I. (1969) Blood flow of the hyperplastic and neoplastic human prostate measured by hydrogen polarography. *Scand. J. Urol. & Nephrol.,* 3, 271-275.

HERRERA, M. A., McCULLOUGH, D., HARRISON, L. and LINK, K. M. (1989) Prostatic urethroplasty results at Bowman Gray School of Medicine. *Sems. in Intervent. Radiol.,* 6, 61-64.

HULBERX, J. C. (1989) Benign prostatic hyperplasia. *Ibid.,* 6, 8-9.

INCROPERA, F. P. and DEWITT, D. P. (1981) *Fundamentals of heat transfer.* Wiley & Sons, New York.

JAIN, R. K. and DUDAR, T. E. (1983) Microcirculatory flow response to hyperthermia (abstract). 31st Ann. Meet. Radiat. Res. Soc., San Antonio, Texas, 26 February-3 March, Abstract Ac-5, p. 8.

KUBAN, D. A., EL-MAHDHI, A. M., SCHELLHAMMER, P. F., and BABB, T. J., (1985), The effect of transurethral prostatic resection on the incidence of osseous prostatic metastasis, *Cancer,* 56, 961-964.

LEVINE, E. S., CISEK, V. J., MULVIHILL, M. N., and COHEN, E. L. (1986), Role of transurethral resection in dissemination of cancer of prostate, *Urology,* 28(3), 179-183.

MACHAN, L., GILL, K. P., ABEL, P., JAGER, H. R., WILLIAMS, G. and ALLISON, D. J. (1989) Prostatic urethroplasty results at the Royal Postgraduate Medical School. *Sems. in Intervent. Radiol.,* 6, 65 71.

MEBUST, W. K., HOLTGREWE, H. L., COCKETT, A. T. K., PETERS, C. P., and the Writing Committee (1989) Transurethral prostatectomy: immediate and postoperative complications. A cooperative study of 13 participating institutions evaluating 3,885 patients. *J. Urol.,* 141, 243-247.

PATEL, U. H., DEFORD, J. A. and BABBS, C. F. (1991) Computer aided design and evaluation of novel catheters for conductive interstitial hyperthermia. *Med. & Biol. Eng. & Comput.,* 29, 25-33.

PENNES, H. H. (1948) Analysis of tissue and arterial blood temperature in the resting forearm. *J. Appl. Physiol.,* 1, 93-122.

SAPOZINK, M. D., BOYD, S. D., ASTRAHAN, M. A., JOZSEF, G. and PETROVICH, Z. (1990) Transurethral hyperthermia for benign prostatic hyperplasia: preliminary clinical results. *J. Urol.,* 143, 944-950.

STROHMAIER, W. L., BICHLER, K. H., FULCHTER, S. H. and WILBERT, D. M. (1990) Local microwave hyperthermia of benign prostatic hyperplasia, *J. Urol.,* 144, 913-917.

VINCENTE, J., CHECHILE, G., SALVADOR, J. and IZQUIERDO, F. (1989) Long-term follow-up of patients with intraurethral prostheses. *Sems. in Intervent. Radiol.,* 6, 82-89.